Structure
Article

Crystal Structure of the Ectodomain Complex of the CGRP Receptor, a Class-B GPCR, Reveals the Site of Drug Antagonism

Ernst ter Haar,[1] Christopher M. Koth,[1,3] Norzehan Abdul-Manan,[1] Lora Swenson,[1] Joyce T. Coll,[1] Judith A. Lippke,[1] Christopher A. Lepre,[1] Miguel Garcia-Guzman,[2] and Jonathan M. Moore[1,*]
[1]Vertex Pharmaceuticals Incorporated, 130 Waverly Street, Cambridge, MA 02139, USA
[2]Vertex Pharmaceuticals San Diego LLC, 11010 Torreyana Road, San Diego, CA 92121, USA
[3]Present address: Genentech, Inc., 1 DNA Way, MS 27, South San Francisco, CA 94080 USA
*Correspondence: jonathan_moore@vrtx.com
DOI 10.1016/j.str.2010.05.014

SUMMARY

Dysregulation of the calcitonin gene-related peptide (CGRP), a potent vasodilator, is directly implicated in the pathogenesis of migraine. CGRP binds to and signals through the CGRP receptor (CGRP-R), a heterodimer containing the calcitonin receptor-like receptor (CLR), a class B GPCR, and RAMP1, a receptor activity-modifying protein. We have solved the crystal structure of the CLR/RAMP1 N-terminal ectodomain heterodimer, revealing how RAMPs bind to and potentially modulate the activities of the CLR GPCR subfamily. We also report the structures of CLR/RAMP1 in complex with the clinical receptor antagonists olcegepant (BIBN4096BS) and telcagepant (MK0974). Both drugs act by blocking access to the peptide-binding cleft at the interface of CLR and RAMP1. These structures illustrate, for the first time, how small molecules bind to and modulate the activity of a class B GPCR, and highlight the challenges of designing potent receptor antagonists for the treatment of migraine and other class B GPCR-related diseases.

INTRODUCTION

CGRP is a 37-amino acid neuropeptide belonging to a family of related hormones that also includes calcitonin, adrenomedullin, and amylin. One of the most potent vasodilators known, CGRP is found widely in both the central and peripheral nervous systems, and is the major neuropeptide of the trigeminovascular system. CGRP is expressed at trigeminal nerve endings that innervate cerebral blood vessels, and this localization, its vasodilatory effect, and other evidence suggest a direct role of CGRP in migraine (Doods et al., 2007; Link et al., 2008). For example, early studies showed CGRP at elevated levels in jugular venous blood, but not in peripheral blood (Goadsby et al., 1990), and infusion of exogenous CGRP into migraine-susceptible patients causes headache and migraine-like disorders (Lassen et al., 2002). Recent data from clinical trials with the CGRP antagonists olcegepant (BIBN409BS6) (Olesen et al., 2004) and telcagepant (MK0974) (Ho et al., 2008a) show that these agents are efficacious in treating acute migraine.

Understanding the mechanisms of CGRP receptor activation by CGRP peptide, and conversely antagonism by small molecules and peptides, is difficult due to the complex nature of the target. CGRP receptor (CGRP-R) consists of two protein components, CLR and RAMP1. CLR, the calcitonin receptor-like receptor, is a class B GPCR. This class, also known as the hormone, or secretin-like receptors, all bind polypeptide hormones of 27–141 amino acids, possess a structured N-terminal extracellular domain (ECD) or ectodomain, a seven helix transmembrane (7-TM) domain, and an intracellular carboxyl terminus. Other members of this class include receptors for secretin, glucagon, vasoactive intestinal peptide (VIP), parathyroid hormone (PTH), corticotropin-releasing factor (CRF), pituitary adenylate cyclase-activating peptide (PACAP), and calcitonin (CTR). Structures of several ECDs have been solved by X-ray crystallography or NMR spectroscopy, and all possess a common $\alpha-\beta-\beta-\alpha$ folding topology stabilized by three conserved disulfide pairs (Grace et al., 2004, 2007; Pioszak et al., 2008; Pioszak and Xu, 2008; Runge et al., 2008; Sun et al., 2007). Several ECD structures have been solved with peptides bound (Grace et al., 2007; Pioszak et al., 2008; Pioszak and Xu, 2008; Runge et al., 2008; Sun et al., 2007); however, no structures have been reported with either small molecule agonists or antagonists bound to any class B GPCR.

A subset of class B GPCRs, including CTR and CLR, form multimeric complexes with receptor activity-modifying proteins, or RAMPs (McLatchie et al., 1998). The three known RAMP proteins all contain a cleavable signal peptide, N-terminal extracellular domain, single transmembrane helix, and an intracellular C-terminal domain. Combinations of the three RAMP proteins with CLR confer specificity for different signaling peptides. For example, the heterodimer consisting of CLR and RAMP1 is specific for CGRP, while CLR/RAMP2 and CLR/RAMP3 are adrenomedullin receptors. In addition, CTR combined with each of the three RAMP proteins forms three distinct amylin receptor subtypes. While both the RAMP (Kuwasako et al., 2003) and CLR (Ittner et al., 2005; Koller et al., 2002) N-terminal sequences clearly determine specificity for peptide agonists, several studies have also implicated them as important determinants for antagonist binding (Hay et al., 2006; Mallee et al., 2002;

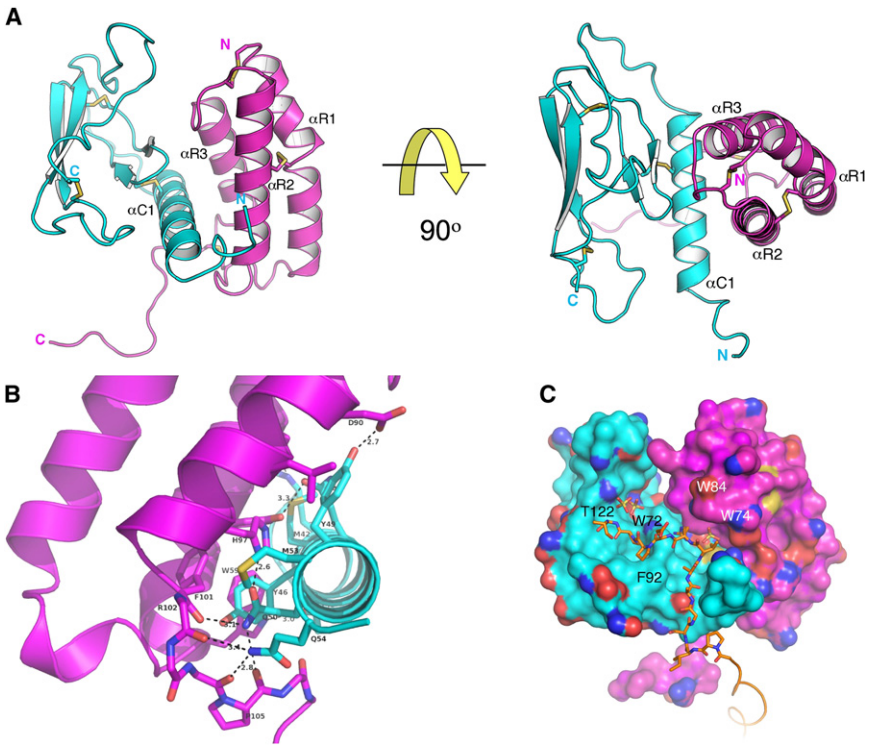

Figure 1. Structure of the CLR/RAMP1 Ectodomain Complex

(A) Ribbon diagram of CLR (cyan) and RAMP1 (magenta). Disulfide bonds are shown in yellow. Helices in RAMP are labeled αR1–αR3, and the single helix in CLR is labeled αC1.

(B) The CLR-RAMP1 interface. Detailed interactions of CLR helix αC1 with helices αR2 and αR3 and the C-terminal loop region (102–108) of RAMP1 are shown. Protein side-chain carbons are colored cyan and magenta for CLR and RAMP1, respectively. Protein heteroatoms are colored: O, red; N, blue; S, yellow.

(C) Surface representation of the CLR/RAMP1 complex. Key residues on RAMP1 are labeled in white, while residues on CLR are labeled in black. Surfaces of charged residues are shown in red (-) and blue (+). The C-terminal tail (amber) of RAMP1 from one symmetry-related CLR/RAMP1 complex binds at the CLR-RAMP1 interface of the adjacent CLR/RAMP1. The C-terminal RAMP1 "tail peptide" sequence shown corresponds to residues 105–117 (PISGRAVRDPPGS). Two sulfate ions bind near CLR Thr122 and one sulfate binds in the hydrophobic pocket defined by RAMP residues Trp74 and Trp84. Formation of the CLR/RAMP1 complex results in a buried surface area of 1032.1 Å^2 for the heterodimer. Details regarding crystallization, structure determination and refinement are provided in the Experimental Procedures and Table 1.

Salvatore et al., 2006). Based on these observations, and previous chemical crosslinking studies (Hilairet et al., 2001), it was suggested that both proteins together form the antagonist binding pocket.

As with most GPCRs, biochemical and biophysical analyses of the CGRP receptor are difficult due to the membrane-bound nature of the target and the lack of an abundant natural source from which protein may be purified. Recombinant expression and purification are complicated further by the functional requirement of a dimeric receptor, and the presence of multiple disulfide bonds in both CLR and RAMP1. To address these challenges, a reductionist approach was used to express and purify a stable, functional binary complex of the extracellular domains of CLR and RAMP1. N-terminal ectodomain constructs of CLR and RAMP1 were expressed separately as inclusion bodies in *Escherichia coli*, but refolded together to form a 1:1 complex. This ectodomain complex was competent to bind CGRP, as well as both peptide and small molecule antagonists (Koth et al., 2010). Here, we report the crystallographic structures of the ectodomain complexes of the CGRP receptor in the unliganded state, as well as with the potent, clinically validated CGRP receptor antagonists olcegepant and telcagepant.

RESULTS AND DISCUSSION

Structure of the CGRP Receptor Ectodomain Complex

The crystal structure of the CLR/RAMP1 ectodomain complex in the unliganded state is shown in Figure 1. In the complex with RAMP1, CLR has an overall fold with some features similar to those found in other class B GPCR ectodomain structures (Grace et al., 2004, 2007; Parthier et al., 2007; Pioszak et al., 2008; Pioszak and Xu, 2008; Runge et al., 2008; Sun et al., 2007). Observable density at the N terminus of CLR begins at residue 29 and forms a helix (labeled αC1) from residues 35–53. This CLR helix packs against helices αR2 and αR3 of the three-helix bundle of RAMP1. The αC1 helix length and positioning in CLR is very similar to that observed for both the PTH receptor (Pioszak and Xu, 2008) and the GIP receptor (Parthier et al., 2007) (Figure 2), but differs considerably from the very short helical stretch seen in the CRFR1 (Pioszak et al., 2008) and CRFR2 (Grace et al., 2004, 2007) receptor ectodomains. A long loop of irregular secondary structure (residues 55–64) follows, leading to a long finger-like motif from residues 65–81. This finger-like structural motif, stabilized by a pair of disulfide bonds between Cys48-Cys74 and Cys65-Cys105, is conserved across all ectodomain structures. At the tip of the finger is Trp 72, a key residue involved in binding small molecule antagonists. Following the Trp finger is a two-stranded antiparallel β sheet. In the orientation shown (Figure 1A), the loop between strands 1 and 2 defines the base of the ligand binding site, and presumably is closest to the 7-TM domain of CLR. While the finger-like motif is common among the class B ECD structures, other elements of secondary structure vary, for example, the lengths of helices (analogous to helix αC1 of CLR), the presence of additional short helical motifs, and the lengths and conformations of loop structures. These features may provide an additional basis for conferring specificity as well as potential sites for allosteric modulation.

The RAMP1 domain contains a three helix bundle, aligned roughly perpendicular to helix αC1 of CLR. Starting from the N terminus, the first and longest of the RAMP1 helices, αR1, spans residues 28–51, but is interrupted by the disulfide bond between

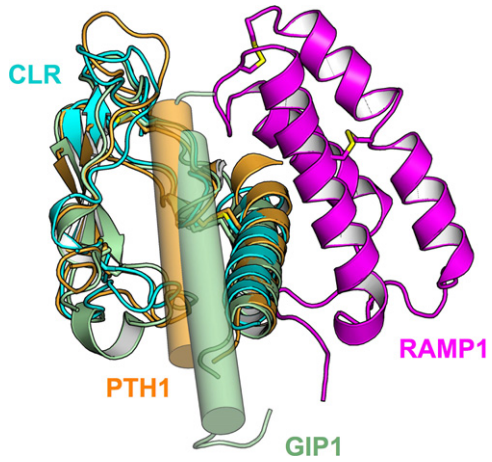

Figure 2. Superposition of CLR/RAMP1 with the Ectodomain Structures of PTH1 and GIP1

PTH1 Receptor (Pioszak and Xu, 2008) (pdb id: 3c4m) and GIP1 receptor (Parthier et al., 2007) (pdb id: 2qkh). PTH (gold) and GIP (green) are each superimposed on CLR (cyan). RAMP1 is shown in magenta and is not used for the alignment. Rmsds for backbone atoms of PTH1-R and GIP1-R ECDs with the CLR ECD are 1.35 and 2.56 Å, respectively. The helical peptides glucose-dependent insulinotropic polypeptide (GIP) and parathyroid hormone (PTH) are shown as transparent cylinders. See also Figure S2.

C40 and C72. Although the backbone dihedral angles are in the α-helical range for all residues in this helix, the backbone carbonyls of residues 37 and 38 do not form intrahelical H-bonds with the backbone nitrogens. Helix αR1 is followed by a short 3-10 helix (residues 53–56) followed by helix αR2 (residues 62–79), a short loop, and helix αR3 (residues 86–101) at the C terminus.

Numerous interactions, both electrostatic and hydrophobic in nature, stabilize the CLR/RAMP1 heterodimer, and occur predominantly between helix αC1 of CLR and helices αR2 and αR3 and the C-terminal loop region (102–108) of RAMP1. Some of the key interactions are shown in Figure 1B. Viewed from the near end of the CLR helix, an extensive hydrogen bonding network is observed involving two CLR Gln side chains. The CLR Gln54 side-chain carbonyl interacts with the backbone amides of RAMP1 Arg102 and Cys104, while the CLR Gln50 side-chain carbonyl bonds with the side-chain and backbone amide groups of RAMP1 residues His97, Phe101, and Pro105, respectively. Additional side-chain-side-chain hydrogen bonding occurs between CLR residues Tyr49 and Gln45 with RAMP1 residues Asp90 (helix αR3) and Tyr66 (helix αR2), respectively. Also visible are hydrophobic interactions between CLR Tyr46 and both RAMP1 Trp59 (loop connecting helix αR2 and helix αR3) and Phe101 (helix αR3). A complete list of CLR-RAMP1 helix-helix interactions is provided in Table 2. The buried surface area arising from complex formation is >1000 $Å^2$ (Figure 1B). Despite this large interaction surface, when compared with the X-ray structure of the RAMP1 homodimer (Kusano et al., 2008), formation of a heterodimer with CLR does not cause a major rearrangement of RAMP1 structural features; the secondary structural elements, disulfide bonds, and interhelical contacts found in the RAMP1 homodimer are largely conserved in the complex with CLR.

It is important to note that although we classify this CLR/RAMP1 binary complex structure as unliganded, examination of the electron density map reveals that eleven C-terminal residues of RAMP1 from one receptor complex occupy part of the ligand binding site of an adjacent receptor complex in the crystal lattice (Figure 1C). This interaction is strictly crystallographic in nature owing to the truncated construct used for crystallization; for a full-length receptor, this sequence would constitute part of the juxtamembrane region. The bound tailpiece, corresponding to residues 109–117, occupies a site primarily on the CLR face, but adjacent to the interface with RAMP1. The peptide runs through a channel beginning near Arg38 of CLR, up toward a deep pocket of hydrophobic residues on RAMP1, then crosses the Trp72 finger of CLR, below the small molecule binding pocket (described in the next section), leaving the C-terminal RAMP1 Ser117 contacting a shallow hydrophobic pocket. A sulfate ion is bound to CLR Thr122 in this complex, but not in liganded complexes. Although the observed protein-protein contacts are not biologically relevant, these interactions may be useful for the design of novel antagonists with alternative binding modes.

Receptor Recognition Elements for Antagonist Binding

The CLR/RAMP1 ECD complex used in this study has been shown, particularly for small molecule and peptide antagonist binding, to be a valid functional surrogate for the full-length receptor complex (Koth et al., 2010). For example, using radioligand binding methods, olcegepant (Figure 3) binds to the full-length receptor with low picomolar affinity (K_D = 45 pM (Schindler and Doods, 2002); K_i = 14 pM (Doods et al., 2000)). Olcegepant also shows high affinity for the ectodomain complex (as measured by surface plasmon resonance), with a dissociation constant below the limit of detection (K_D < 20 nM) (Koth et al., 2010). Crystals of olcegepant with the ectodomain complex contained two CLR/RAMP1 complexes per asymmetric unit. These crystals were unusual in that olcegepant only bound to one of the two CLR/RAMP1 pairs, with the second ligand binding site occupied by the C terminus of the RAMP1 from an adjacent complex. The two binding sites in this crystal form were very similar structurally, with pairwise root mean square deviations (rmsds) of 1.48 Å between the two complexes in the asymmetric unit, and 1.18 Å for atoms within <4.5 Å of the bound olcegepant molecule (superpositions are shown in Figure S1 available online). The structure of olcegepant bound to the CGRP receptor ectodomain complex (Figure 4) reveals the key drug-protein interactions that contribute to antagonist potency. The drug molecule binds in an extended conformation (Figures 4C and 4D), stretching ~18 Å from a hydrogen bond donor site at Thr122 of CLR, across the interface with RAMP1, and deep into a hydrophobic binding pocket formed by helix αC1 of CLR and helix αR2 of RAMP1. RAMP1 residues Trp74 (helix αR2) and Trp84 (in the loop connecting RAMP1 helices αR2 and αR3) form the ceiling and back surface of the hydrophobic binding pocket (Figure 4D). The quinazolinone moiety of olcegepant forms a hydrogen bond donor-acceptor pair with the backbone NH and carbonyl of CLR Thr122. The side chain of CLR Trp72 undergoes a rotation of ~70° compared with the unliganded complex, forming a "Trp shelf" on which the piperidine ring of olcegepant stacks. Olcegepant branches at the

Table 1. X-Ray Refinement Statistics

	SeMet High Resolution	SeMet Peak	Olcegepant	Telcagepant
Wavelength	1.000	0.9804		
Space group	P3221	P3221	C2221	C2221
Cell dimensions	a = b = 118.2 c = 225.8	a = b = 118.2 c = 225.8	a = 73.3 b = 119.1 c = 137.2	a = 77.9 b = 118.2 c = 133.3
No. of reflections	130,149	321,993	340,718	310,841
No. of unique reflections	39,161	34,485	30,514	10,399
Completeness (%)	84.9 (36.0)	79.6 (28.5)	86.9 (51.5)	73.6 (12.1)
Rmerge[a]	0.065 (0.319)	0.099 (0.403)	0.073 (0.424)	0.066 (0.438)
I/sigma	23.8 (2.6)	21.3 (1.7)	20.2 (2.1)	18 (1.6)
Redundancy	3.3 (2.4)	3.3 (2.4)	4.6 (3.1)	4.1 (1.3)
Resolution (Å)	2.79	3.00	2.10	2.9
R_{work}/R_{free}	0.21/0.24	NA	0.21/0.23	0.23/0.27
Number of atoms	5537	NA	3118	2832
Protein	5404	NA	2902	2698
Ligand/ion	221	NA	216	134
Water	53	NA	131	40
B factors Wilson/Mean	64.2/97.4	NA	32.8/43.1	62.7/91.53
Rmsd				
Bond lengths (Å)	0.01	NA	0.01	0.01
Bond angles (°)	1.06	NA	1.02	1.03
Ramachandran plot (%)				
Most favored	92.5	NA	93.4	94.1
Additionally allowed	7.1	NA	6	5.9
Generously allowed	0.3	NA	0.6	0
Disallowed	0	NA	0	0
SAD structure solution				
Resolution cutoff (Å)		6.0		
No. anomalous sites found		9 (of 12)		
Figure of merit (to 3.2 Å)		0.212		
Phasing power (to 3.2 Å)		0.717		

[a] $R_{sym} = \Sigma\Sigma_j |I_j - < I > |/\Sigma\Sigma_j I_j$.

amide linkage, extending both to the rear of the binding pocket, where the hydroxyl of the dibromotyrosyl group interacts via a water-mediated hydrogen bond with both the CLR αC1 (Arg38 ε-NH) and RAMP1 αR2 (Arg67 CO) helices, and toward the solvent-exposed surface, where the carbonyl of the second amide-linkage forms a hydrogen bond with the indole NH of CLR Trp72. The lysine 6-amino terminus of olcegepant forms a salt bridge with the side-chain carboxyl of RAMP1 Asp72, while the indole of RAMP1 Trp74 stacks with the aliphatic portion. Finally, the terminal pyridyl stacks with the aromatic ring of CLR Phe92, while also making a hydrogen bond with the side-chain carboxyl of CLR Asp94.

While it is clear that multiple ligand:protein interactions contribute to the subnanomolar potency of olcegepant, this is achieved with a relatively high molecular weight molecule (MW = 870 Da). Based on the typical physicochemical properties of large drug molecules, it is not surprising that olcegepant is not orally bioavailable. Alternatively, telcagepant (MW = 566 Da) (Figure 3), has demonstrated superior pharmacokinetic properties (Paone et al., 2007), possessing oral bioavailability and efficacy at several doses (Ho et al., 2008a, 2008b). With K_D = 1.9 nM (Moore et al., 2009), telcagepant is not as potent against full-length receptor as olcegepant, but binds with K_D < 20 nM to the ectodomain complex (Koth et al., 2010). Although initial attempts to grow co-crystals of telcagepant with the ectodomain complex failed, we were able to use the crystals of olcegepant/CLR/RAMP1 and soak telcagepant into the unoccupied ligand binding site of the second CLR/RAMP1 heterodimer in the unit cell (displacing the RAMP1 C-terminal peptide). The structure of telcagepant bound to the CGRP ectodomain complex is shown in Figure 5A. Despite its lower MW, telcagepant maintains a similar binding topology to olcegepant, spanning the ~18 Å distance from the Thr122 hydrogen bond donor-acceptor site on CLR to the hydrophobic pocket on RAMP1. A superposition of the two ligands in the CLR/RAMP1 binding site is shown in Figure 5C. The structure reveals a slightly different topology at

Table 2. Helix-Helix and Helix-Loop Interactions between CLR and RAMP1

	No Ligand	Ligand
Hydrogen bond	T43 - W59 Y49 - D90 Q50 - H97, F101, P105 Q54 - C104, R102 Q45 – Y66	T43 - W59 Y49 - D90 Q50 - H97, F101, P105 Q45 – Y66 T68 – D90 E47 - G108 N39 - R67
Hydrophobic interaction	M42 - Y66, A70, R67 Y46 - W59, F101, Y66 Y49 - F93, L94, H97 M53 - L94, G98, R102 R119 - F83	M42 - Y66, A70, R67 Y46 - W59, F101, Y66, G108 Y49 - F93, L94, H97 M53 - L94, G98, R102 R119 - F83
Salt Bridge	R38 - D71	R38 - D71

For each pair, the first residue listed is from CLR; the second (or additional) residues are from RAMP1. The olcegepant-liganded structure (2.1 Å resolution) was used for the analysis. In that complex, there are two CLR/RAMP1 complexes in the asymmetric unit, with the small molecule binding site of one complex occupied by olcegepant, and the other vacant.

the hydrogen bond donor-acceptor site (Figure 5D), where the azabenzimidazolone ring system of telcagepant forms an additional weak hydrogen bond with the backbone carbonyl of CLR Thr122. As in olcegepant, the piperidyl moiety forms an edge-to-face stack with CLR Trp72. The carbonyl of the seven-membered caprolactam ring forms a weak hydrogen bond with the indole NH of CLR Trp72, analogous to the amide group in olcegepant. While binding of the dibromotyrosyl group of olcegepant relies on both hydrophobic and electrostatic interactions, binding of the difluorophenyl group of telcagepant appears to be primarily hydrophobic in nature. Here, RAMP1 Trp74 and RAMP1 Trp84 similarly frame the hydrophobic pocket, with the difluorophenyl reaching deeper into the pocket than the dibromotyrosine, displacing a bound water molecule and making hydrophobic contacts with the side chain of CLR Met42, a residue previously implicated in telcagepant binding (Miller et al., 2010). Additional hydrophobic contacts arise between the ligand trifluoroethyl and the side chain of CLR Ile41.

The efficiency of ligand:protein interactions can differentiate a potent antagonist with poor pharmacokinetic properties from an orally bioavailable drug molecule. Although telcagepant (K_D = 1.9 nM (Moore et al., 2009); MW = 566 Da) is not as potent as olcegepant (K_D = 45 pM (Schindler and Doods, 2002); MW = 870 Da), at a significantly lower MW it makes fewer, but more productive contacts with the receptor ectodomain. For telcagepant, increased binding efficiency results from an additional hydrogen bond from the azabenzimidazolone group at the CLR Thr-122 site, as well as from replacement of the dibromotyrosyl group of olcegepant with a lower MW difluorophenyl group. The difluorophenyl extends deeper into the RAMP1 hydrophobic pocket and makes additional hydrophobic contacts with CLR and RAMP side chains, while displacing a bound water molecule, potentially enhancing both the enthalpic and entropic components, respectively, of the ligand binding energy (compared with olcegepant) for this receptor subsite.

Comparison with Other Class B GPCR Ectodomains and Ligand Binding Sites

The structure of CLR in the ectodomain complex aligns well with other class B GPCRs. The alignment is particularly strong for the GIP and PTH receptor domains, which possess a helix similar in length to helix αC1 of CLR (Figure 2). The disulfide-stabilized finger-like motif is also well defined and conserved across all the published structures. It is difficult to predict whether CGRP binds in a helical conformation similar to the peptides bound to the GIP (Runge et al., 2008), PTH (Pioszak and Xu, 2008), CRFR1 (Pioszak et al., 2008), CRFR2 (Grace et al., 2007), and PAC1 (Sun et al., 2007) receptors. Although PTH, GIP, and astressin bind with the same approximate helix orientation, they occupy different positions on one face of the ECD, whereas PACAP binds PAC1-R on the opposite face (Figure S2). The olcegepant and telcagepant crystal structures suggest that a PACAP-like peptide binding orientation can be ruled out, since these antagonists are competitive with the functional mode of binding for CGRP. Similarly, an astressin-like conformation (Figure S2) is less likely since it is hard to envision how RAMP1

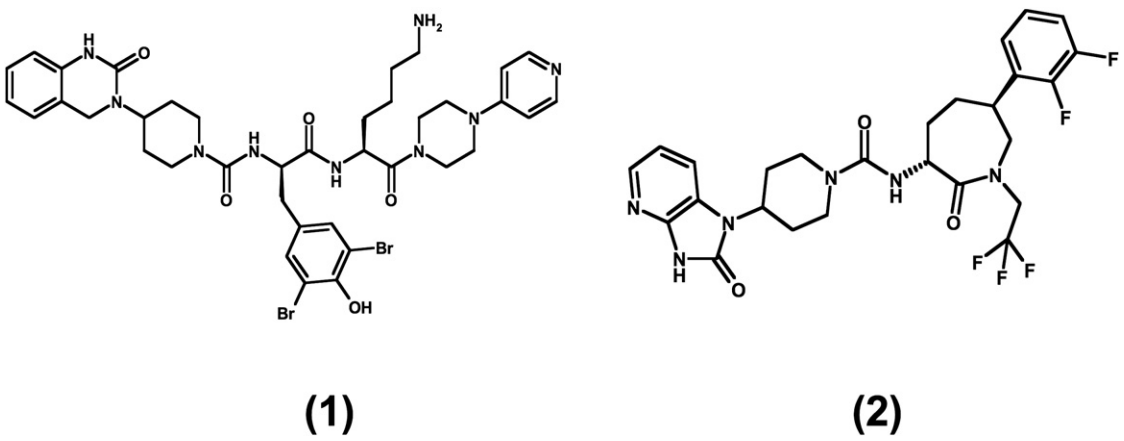

Figure 3. Chemical Structures of Olcegepant and Telcagepant
Olcegepant (Compound **1**) is shown on the left and telcagepant (Compound **2**) on the right.

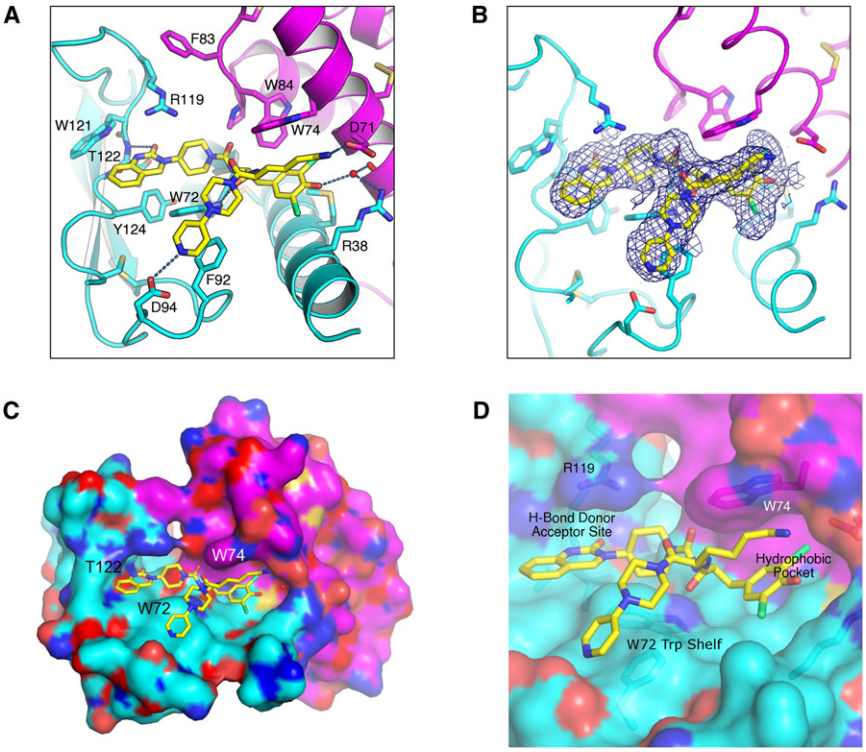

Figure 4. Structure of the Olcegepant/CLR/RAMP1 Liganded Complex.

(A) Olcegepant (yellow) binds at the interface of CLR (cyan) and RAMP1 (magenta). Dashed dark lines indicate hydrogen bonds to the backbone of Thr122 and side chain of Asp94 on CLR, the side chain of RAMP1 Asp71, and a water-mediated hydrogen bond at the CLR-RAMP1 interface involving CLR Arg38 and RAMP1 Arg67.

(B) The Fo-Fc electron density map contoured at 3σ is superimposed on the structure of olcegepant (yellow).

(C) CLR/RAMP1 is shown in surface representation, olcegepant is shown in stick representation. Coloring for olcegepant: C, yellow; O, red; N, blue; Br, green.

(D) Detail of olcegepant binding pocket.

See also Figure S1.

could confer specificity at such a long distance from the peptide. A more likely peptide binding orientation might resemble that of GIP or PTH, where the peptide C terminus comes into close contact with the Phe83-Pro85 loop of RAMP1. In such an orientation, RAMP1-peptide interactions could dictate peptide (CGRP versus AM) selectivity and would easily be blocked by olcegepant or telcagepant.

Utility of the CLR/RAMP1 Ectodomain Structure for Ligand Design

Although we have taken a reductionist approach in crystallizing the soluble ectodomain complex rather than the full-length GPCR-accessory protein complex, the observation that the CLR/RAMP1 heterodimer binds olcegepant and telcagepant with low nanomolar or tighter affinity (Koth et al., 2010) gave us confidence that the ectodomain complex can serve as a useful model for drug lead optimization. Fortunately, much SAR work has been published, which allows a retrospective analysis of compound potency as it relates to the key structural features of the CLR/RAMP1 ectodomain complex. Specifically, increases in potency found for compounds on the optimization path to olcegepant (Rudolf et al., 2005) (Figure 6A) and telcagepant (Paone et al., 2007; Shaw et al., 2007) (Figure 6B) can be rationalized based on the quality of interactions of the small molecule with pharmacophore recognition sites on CLR/RAMP1. In the case of olcegepant, compounds were selected to optimize electrostatic interactions with the hydrogen bond donor-acceptor site at CLR Thr122, while for telcagepant, altering the positioning and stereochemistry of substituents on the caprolactam ring resulted in increased potency through better access to the RAMP1 hydrophobic pocket.

Rudolf et al. (2005) provide a detailed description of the chemical design strategies used leading to the synthesis of olcegepant. Using the ligand-protein interactions and conformation of olcegepant bound to CLR/RAMP1 (Figures 4A and 5D) as a basis for evaluating each ligand, the lower potencies of compounds **12** and **16** (Figure 6A) can be explained by differences in the interactions these compounds make with the receptor. For example, first-generation lead compound **12** lacks both the piperidyl amide (important for hydrophobic stacking with CLR Trp72) and the hydrogen bond donor-acceptor pair found in olcegepant. The ethyl linker connecting the 2-methoxyphenyl group and amide nitrogen of compound **12** (IC_{50} = 1 μM) is not long enough to position the former group appropriately for hydrogen bonding with the Thr122 backbone carbonyl and amide NH. Without these key interactions, it is not surprising that this compound would be a weak binder. Alternatively, compound **16** (IC_{50} = 44 nM) possesses the same piperidyl amide linker as in olcegepant but is linked to a 2(*3H*)-benzoxazolone ring system containing two hydrogen bond donors (shown schematically in Figure 6A). Here, the piperidyl amide can form a hydrophobic stacking interaction with Trp72 of CLR, and is the correct length for positioning the benzoxazolone ring oxygen near the Thr122 backbone NH. This single hydrogen bonding interaction, along with a better hydrophobic stacking interaction due to the piperidyl versus ethyl linker, results in a 22-fold increase in potency compared to compound **12**. The most potent compounds (IC_{50} < 5 nM) in this series, including the exquisitely potent olcegepant (Figure 6A, compound **19**) (IC_{50} = 30 pM), possess a piperidyl amide, extending to a donor-acceptor pair that forms hydrogen bonds with the Thr122 backbone carbonyl and amide groups (Figures 5D and 6).

Several papers describe the evolution of the caprolactam class of CGRP antagonists leading to the clinical compound telcagepant (Paone et al., 2007; Shaw et al., 2007). The first study (Shaw et al., 2007) describes optimization of the stereochemistry and substitution pattern on the central caprolactam

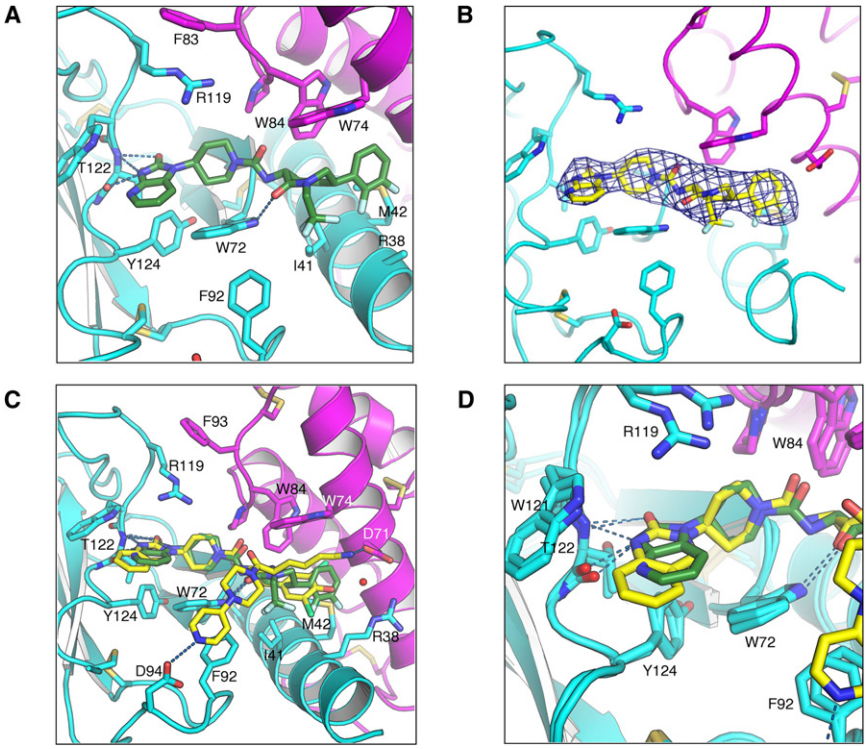

Figure 5. Structure of the Telcagepant/CLR/RAMP1 Liganded Complex and Comparison of Olcegepant and Telcagepant Binding

(A) CLR/RAMP1 is shown in ribbon representation; telcagepant is shown in stick representation. Coloring for telcagepant: C, green; O, red; N, blue; S, yellow; F, light blue. Protein side-chain carbons are colored cyan and magenta for CLR and RAMP1, respectively. Protein heteroatoms are colored: O, red; N, blue; S, yellow.

(B) The Fo-Fc electron density map contoured at 3σ is superimposed on the structure of telcagepant. Coloring for telcagepant: C, yellow; O, red; N, blue; F, light blue.

(C) Overlay of the structures of olcegepant and telcagepant at the antagonist binding site. Both ligands are shown in stick representation. Coloring for olcegepant: C, yellow; O, red; N, blue; Br, green.

(D) Details of hydrogen bond donor-acceptor interactions for olcegepant and telcagepant. Dashed dark lines indicate hydrogen bonds to the backbone of Thr122 on CLR.

group. Specifically, the hydrogen bond donor-acceptor group was limited to quinazolinone (as found in olcegepant), and the stereochemistry and position of the phenyl group on the seven-membered 1-cyclopropylmethyl caprolactam ring were then modified. Several 7-, 6-, and 5-phenyl-substituted compounds were synthesized. The 7-phenyl-substituted compounds were the least active, and the most potent of these is shown in Figure 6B (top). Examination of the X-ray structure of telcagepant bound to the CLR/RAMP1 binding pocket suggests that changing the position of ring attachment from the 6- to either a 7- or 5- position on the caprolactam would no longer provide an optimal vector for this group to access the RAMP1 hydrophobic pocket. In fact, the 7-phenyl caprolactam would not be able to access the pocket at all, which explains the low affinity observed for this compound (K_i = 689 nM) (Figure 6B, left). The 6-phenyl-substituted caprolactam (*3R,7S* stereochemistry) (Figure 6B, middle), however, showed ~28-fold improvement in potency. 5-Phenyl-substituted compounds, while still active, displayed a slight loss in potency. Importantly, the structures can easily explain the absolute requirement for a *3R* configuration at C-3 of the caprolactam ([3*R*,6*S*], K_i = 25 nM; [3*S*,6*R*], K_i = 5828 nM) (Shaw et al., 2007). Inversion of the stereochemistry to a *3S,6R* configuration results in the caprolactam favoring pseudoaxial placement of either the amide or the phenyl substituent versus the linear pseudoequatorial placement preferred by the (*3R,6S*) diastereomer. The result is a highly strained caprolactam ring that is unable to adopt an extended conformation required for placement of the caprolactam C6 phenyl in the CLR/RAMP1 hydrophobic pocket.

The CLR/RAMP1 Ectodomain Structures as a Context for Interpretation of Functional Data

Previous studies of ectodomain function using full-length receptor have examined the species selectivity of CGRP antagonists, as well as antagonist binding specificity mediated by different RAMP subtypes. Mutational and deletion analyses have identified residues critical for receptor function, including heterodimer formation, transport to the plasma membrane and antagonist binding. Given this large body of functional data, it is useful to assess how the current structures support our current understanding of CGRP receptor biology.

For example, ^{125}I-CGRP radioligand binding assays indicated both olcegepant and telcagepant exhibit a higher affinity for the human CGRP receptor than the rat receptor. The selectivity observed is >100-fold for olcegepant (Doods et al., 2000), and >1500-fold for telcagepant (Salvatore et al., 2008). For olcegepant, this has been attributed to a sequence difference at RAMP1 residue 74 (Hay et al., 2006; Mallee et al., 2002), which is a tryptophan in primates, but a lysine residue in rat and mouse. The ectodomain complex structure provides a clear rationale for the observed selectivity. RAMP1 Trp74, in the orientation shown (Figures 4C, 4D, and 5A), forms the "ceiling" of the hydrophobic pocket. Replacement of this residue with a lysine would remove a key component of the RAMP1 hydrophobic pocket, both reducing the total ligand-protein hydrophobic surface, and by nature of the longer, charged side chain, sterically hinder access to the binding pocket. While olcegepant has additional functional groups, such as the piperazylpiperidine and 6-aminohexyl moieties, which might compensate for the decreased binding at RAMP1 Trp74, the smaller telcagepant molecule does not, and this could account for the greater observed difference in affinity for telcagepant between the human and rodent receptors. The structure of CLR/RAMP1 may also explain the exquisite selectivity of olcegepant for the CGRP receptor versus the

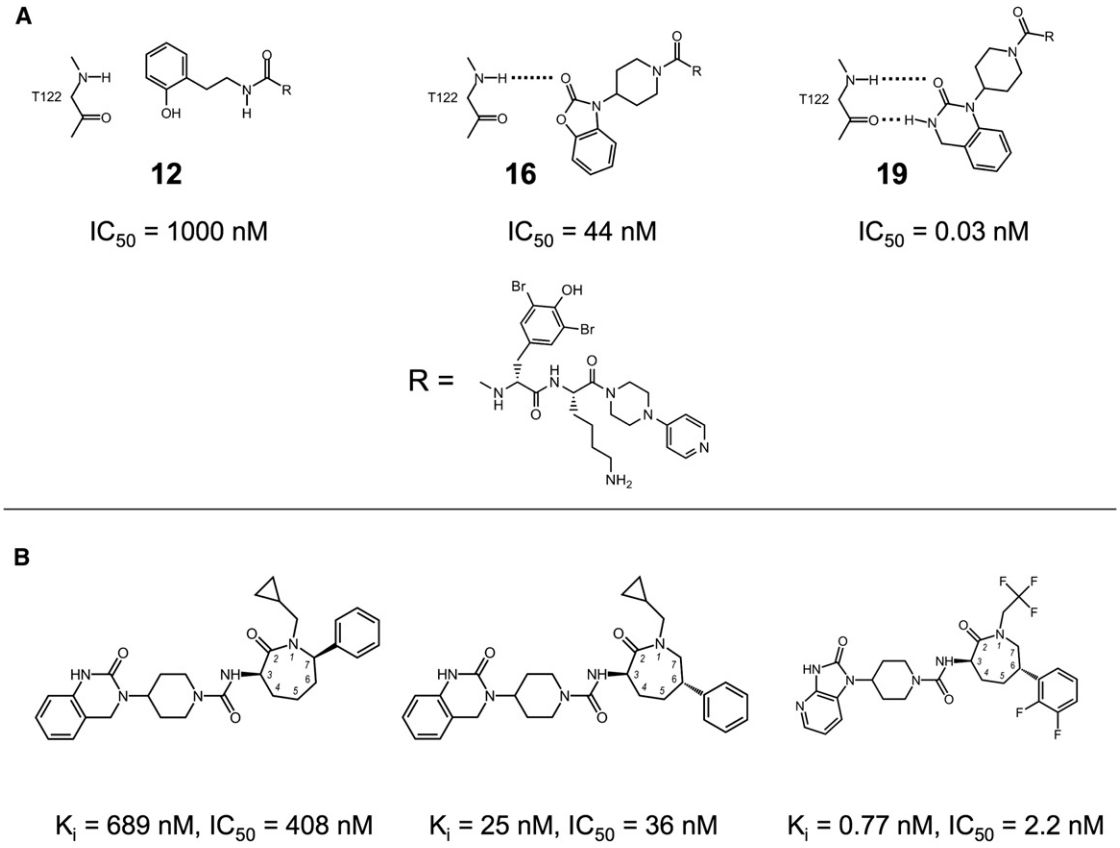

Figure 6. Structure-Activity Relationships for Olcegepant and Telcagepant Lead Optimization

(A) SAR of olcegepant derivatives. Compounds are labeled with the compound numbers listed in Table 1 of Rudolf et al. (2005). Two dimensional cartoon diagrams show putative hydrogen bonding schemes for each compound.

(B) SAR of telcagepant derivatives. K_i and IC_{50} values are taken from Shaw et al. (2007) and Paone et al. (2007). The left and middle structures correspond to Compounds **16** and **20** from Shaw et al. (2007), while the compound on the right is compound **38** (telcagepant) from Paone et al. (2007).

AM_1 (CLR/RAMP2) and AM_2 (CLR/RAMP3) receptors (Hay et al., 2003). While RAMP1 contains a Trp at position 74, RAMP2 and RAMP3 both contain a nonconservative Glu. Other RAMP1 residues (Ala70, Asp71, His75, Phe83, Trp84, and Pro85) also contact olcegepant and may play a minor role in conferring selectivity, but these residues are either identical or conserved across the three RAMP protein sequences. This strongly implicates residue 74 as the key determinant of olcegepant selectivity for the CGRP receptor.

The structures also provide a deeper understanding of previous mutational and deletion analyses with CLR and RAMP1. Several studies have implicated CLR residues (23–60) as necessary for heterodimer formation and transport of the CLR/RAMP1 complex to the plasma membrane (Barwell et al., 2010; Ittner et al., 2005). In one study (Ittner et al., 2005), a chimeric receptor was constructed where homologous residues (29–104) of PTH receptor were changed to those found in CLR (residue 23–60), resulting in CLR/RAMP1 heterodimerization and cotransport to the plasma membrane. In another study, alanine scanning mutagenesis was used to identify residues involved in CGRP binding, cell surface expression, and receptor internalization (Barwell et al., 2010). In the latter work, Gln45Ala and Tyr49Ala significantly impaired cell surface expression. The CLR construct used in the present crystallographic structure determination consisted of residues 23–133, with observable electron density starting at residue 34. Residues 34–60 are highlighted in red in Figure S3 and encompass all of helix αC1 as well as part of the following loop. Contacts between helix αC1 (the single helix in CLR) and helices αR2 and αR3 of RAMP account for most of the buried surface in the heterodimer, and thus are the primary structural elements driving dimerization with RAMP1. Mutations affecting the helix-helix interface, such as Gln45Ala and Tyr49Ala (Barwell et al., 2010), would be expected have profound consequences on the assembly of a functional CLR/RAMP1 complex.

Deletion mutagenesis of RAMP1 (Kuwasako et al., 2003) has similarly identified residues spanning helix αR3 as critical for receptor function. The deletion mutants studied (Figure S4) formed heterodimers and were transported to the cell surface but did not bind ^{125}I-CGRP and were not functional in a cell-based cAMP assay. Deletion of segments of RAMP1 helix αR3 (Δ91-94, Δ96-100) and the loop near the critical disulfide at Cys104 (Δ101-103), would cause disruptions of regular helical secondary structure and severe distortions of the geometry at the putative peptide binding site, including Trp 84, which also helps form the antagonist binding pocket. However, key contacts for heterodimerization between RAMP helix αR2 and

CLR helix αC1 would be preserved, enabling normal transport of CLR/RAMP1 to the cell surface.

In summary, we have used a reductionist approach to crystallize the complex of the extracellular domains of CLR and RAMP1. The structures, the first determined for a class B GPCR with a RAMP protein, reveal how the extracellular domain of the accessory protein binds and modulates the antagonist-binding activities of CLR. Moreover, the structures provide a basis for modeling the interactions of other RAMP proteins with this important therapeutic class B subfamily.

The structures of the important clinical antagonists olcegepant and telcagepant bound to the CLR/RAMP1 ECD complex represent the first for any small molecules bound to a class B GPCR. As such, they provide the first models for structure-based design of new CGRP receptor-targeted pain therapeutics, and clearly illustrate why CGRP antagonist design has been such a daunting drug design problem. In order to meet desired potency and receptor selectivity criteria, antagonist molecules must be of sufficient length to span the distance between the hydrogen bond donor-acceptor subsite on CLR and the hydrophobic pocket on RAMP1. Antagonism via an olcegepant or telcagepant-like binding mode thus imposes a minimum molecular weight requirement. Beyond potency, migraine drugs must also possess physical properties consistent with the desired pharmacokinetic profile. However, such drug-like properties are historically difficult to achieve as molecular mass increases. Although the physicochemical properties for the ideal CGRP receptor-targeted migraine therapeutic run counter to the stringent pharmacophore requirements of the receptor binding site, subnanomolar antagonists with MW as low as 460 Da have been reported (Stump et al., 2009; Theberge et al., 2008), although none have been successful in a clinical setting.

Despite lacking the juxtamembrane and transmembrane domains of CLR and RAMP1, the crystallographic models provide an appropriate context for interpretation of previously reported studies examining chemical structure-activity relationships (SAR), species selectivity, and antagonist binding specificity. The structures also reinforce the conclusions of mutational and deletion analyses that identify residues critical for receptor function, including heterodimer formation, transport to the plasma membrane and antagonist binding.

In conclusion, the structures presented provide insight into the molecular mechanism of CGRP receptor antagonism and establish a new framework for addressing the formidable challenges in structure-based design of CGRP-directed pain therapeutics.

EXPERIMENTAL PROCEDURES

Purification and Refolding of CLR/RAMP1 Extracellular Domains

Details of cloning, expression, refolding, and purification of the CLR and RAMP1 extracellular (ECD) domain complex have been published elsewhere (Koth et al., 2010). In brief, ectodomain constructs for CLR_{23-133} and $RAMP_{26-117}$ were cloned into pET28b with an N-terminal hexahistidine tag followed by a thrombin cleavage site. Proteins were expressed in Rosetta DE3 cells by induction (at AU_{600} of 0.5–0.8) with 0.5 mM isopropyl-b-D-thiogalactopyranoside for 3 hr at 37°C. The selenomethionine-labeled protein complex was prepared by growing cells in M9 SeMET high-yield media (MD045004-12L) purchased from Shanghai Medicilon Inc. (Shanghai, China). After cell harvest and lysis, inclusion bodies were prepared and solubilized in 6 M guanidine hydrochloride containing 100 mM DTT, 50 mM sodium phosphate (pH 8.0). Following dialysis to remove DTT, the proteins were co-refolded to generate the $CLR_{23-133}/RAMP_{26-117}$ ECD complex by mixing equimolar amount at a concentration of 0.1–0.2 mg/ml and dialyzed in a buffer containing 1 M arginine, 50 mM sodium phosphate (pH 8.0), and 5 and 1 mM reduced and oxidized glutathione, respectively. A final dialysis was performed to remove arginine. The supernatant was centrifuged and filtered before resolving by anion exchange, and the co-eluted CLR/RAMP1 was pooled and loaded on an S200 gel filtration column. The purified complex was pooled and concentrated to 15–20 mg/ml for crystallization.

Crystallization, Structure Determination, and Analysis

Crystals were grown using the hanging drop vapor diffusion method over a reservoir containing 1–1.3 M ammonium sulfate, 6%–8% dioxane, 60–80 mM MES (pH 6.5; 60%–80% Classics #50, Hampton Research, Aliso Viejo, CA), plus 10 mM Tris (pH 8.5) and 200 mM sodium nitrate. Crystals appeared in about 2 weeks and were typically harvested after 4 weeks. To prepare the crystals for data collection, they were transferred to 2.1 M sodium malonate (pH 7.0) for approximately 5 min and subsequently frozen in liquid nitrogen. The diffraction data was collected at beamline 5.0.2 of the Advanced Light Source in Berkeley CA. The diffraction data were merged and scaled using HKL2000. The crystals belonged to the space group P3221 but were partially twinned with a twinning fraction of 0.3. The diffraction intensities were detwinned using CCP4's Detwin program. Two data sets were used for structure determination: 0.9804 Å (peak), and 1.0 Å (high-resolution data set). Initial seleno-methionine sites were found with the Se-Met peak data set at 6 Å resolution cutoff using ShelXD. Subsequently, autoSHARP was used (using the Se-Met peak data set at 3.2 Å) to optimize the seleno-methionine sites. The phasing statistics showed that the initial phase information extended to 5.8 Å. This resolution was used as the starting point for density modification and phase extension by autoSHARP. The obtained phases were then used to calculate a 2.8 Å electron density map with the Se-Met High Resolution data set for model building.

Subsequent rounds of building in Quanta and Coot and refinement in autoBUSTER resulted in a final model that contained four CLR/RAMP1 heterodimers in the asymmetric unit of which one was very disordered.

To obtain crystals of the CLR/RAMP1 complex with olcegepant, the compound was mixed with unlabeled CLR/RAMP1 complex prior to crystallization in a 1:4 (protein: compound) molar ratio. Crystals were obtained by mixing 0.6 μl protein with 0.3 μl reservoir solution containing 1–1.3 M ammonium sulfate, 6%–8% dioxane, 60–80 mM MES (pH 6.5; 60%–80% Classics #50, Hampton Research, Aliso Viejo, CA), plus 0.4 M potassium thiocyanate. The crystals appeared after approximately 3 weeks and were typically harvested after 6 weeks. Prior to data collection, the crystals were transferred to 2.1 M sodium malonate (pH 7.0) for about 5 min and subsequently frozen in liquid nitrogen. In order to obtain the complex of CLR/RAMP1 with telcagepant, crystals of the olcegepant CLR/RAMP1 complex were transferred to a mixture containing 2.1 M sodium malonate (pH 7.0) and 0.2 mM telcagepant (dispensed from a 10 mM DMSO stock solution). The crystal was soaked for approximately 16 hr prior to freezing in liquid nitrogen. The data was collected at beamline 5.0.2 (olcegepant) and 5.0.3 (telcagepant) of the Advanced Light Source in Berkeley, CA, indexed, and scaled in HKL2000 and the structure was solved by molecular replacement using unliganded CLR/RAMP1 as the starting model. The crystals belonged to the space group C2221 with two CLR/RAMP1 heterodimers in the asymmetric unit; however, only one of them contained an olcegepant molecule in the ligand-binding site. The crystals that were soaked with telcagepant contained olcegepant in one ligand binding site, and telcagepant in the other. After several rounds of refining in autoBUSTER and rebuilding in Coot a final structure was obtained with a R/Rfree of 0.21/0.23 (olcegepant) and 0.23/0.27 (telcagepant). Structure alignment of CLR with other class B GPCRs was calculated in Pymol (Delano Scientific LLC, Palo Alto, CA). Buried surface area was also determined in Pymol and calculated as Buried Surface $Area_{COMPLEX} = [(AREA_{RAMP1} + AREA_{CLR}) - AREA_{COMPLEX}]/2$.

ACCESSION NUMBERS

Atomic coordinates and structure factors have been deposited in the Protein Data Bank under PDB ID code 3N7P (unliganded), 3N7R (complex with telcagepant), and 3N7S (complex with olcegepant).

SUPPLEMENTAL INFORMATION

Supplemental Information includes four figures and can be found with this article online at doi:10.1016/j.str.2010.05.014.

ACKNOWLEDGMENTS

We thank Marc Jacobs and William Markland for scientific discussions, Guy Bemis and Govinda Rao for assistance with modeling, and Debbie Hay and Patrick Sexton for critical reading of the manuscript. We thank the Vertex-San Diego and Vertex-Cambridge Chemistry teams for synthesis of the ligands used in this study. We thank John Thomson for support of the Membrane Protein Research Initiative. Portions of this research were conducted at the Advanced Light Source, a national user facility operated by Lawrence Berkeley National Laboratory, on behalf of the U.S. Department of Energy, Office of Basic Energy Sciences. E.t.H. grew crystals, collected and analyzed data, and solved the structures; C.M.K. and N.A.-M. devised and implemented the protein refolding and purification strategy; L.S. grew crystals; J.T.C. refolded and purified protein; J.A.L. did cloning; C.A.L. carried out biophysical measurements and edited the manuscript; M.G.-G. and J.M.M. designed the research project; J.M.M. led the research project and wrote the manuscript. All authors discussed the results and commented on the manuscript.

Received: April 4, 2010
Revised: May 21, 2010
Accepted: May 25, 2010
Published: September 7, 2010

REFERENCES

Barwell, J., Miller, P.S., Donnelly, D., and Poyner, D.R. (2010). Mapping interaction sites within the N-terminus of the calcitonin gene-related peptide receptor; the role of residues 23-60 of the calcitonin receptor-like receptor. Peptides *31*, 170–176.

Doods, H., Hallermayer, G., Wu, D., Entzeroth, M., Rudolf, K., Engel, W., and Eberlein, W. (2000). Pharmacological profile of BIBN4096BS, the first selective small molecule CGRP antagonist. Br. J. Pharmacol. *129*, 420–423.

Doods, H., Arndt, K., Rudolf, K., and Just, S. (2007). CGRP antagonists: unravelling the role of CGRP in migraine. Trends Pharmacol. Sci. *28*, 580–587.

Goadsby, P.J., Edvinsson, L., and Ekman, R. (1990). Vasoactive peptide release in the extracerebral circulation of humans during migraine headache. Ann. Neurol. *28*, 183–187.

Grace, C.R., Perrin, M.H., DiGruccio, M.R., Miller, C.L., Rivier, J.E., Vale, W.W., and Riek, R. (2004). NMR structure and peptide hormone binding site of the first extracellular domain of a type B1 G protein-coupled receptor. Proc. Natl. Acad. Sci. USA *101*, 12836–12841.

Grace, C.R., Perrin, M.H., Gulyas, J., Digruccio, M.R., Cantle, J.P., Rivier, J.E., Vale, W.W., and Riek, R. (2007). Structure of the N-terminal domain of a type B1 G protein-coupled receptor in complex with a peptide ligand. Proc. Natl. Acad. Sci. USA *104*, 4858–4863.

Hay, D.L., Howitt, S.G., Conner, A.C., Schindler, M., Smith, D.M., and Poyner, D.R. (2003). CL/RAMP2 and CL/RAMP3 produce pharmacologically distinct adrenomedullin receptors: a comparison of effects of adrenomedullin22-52, CGRP8-37 and BIBN4096BS. Br. J. Pharmacol. *140*, 477–486.

Hay, D.L., Christopoulos, G., Christopoulos, A., and Sexton, P.M. (2006). Determinants of 1-piperidinecarboxamide, N-[2-[[5-amino-l-[[4-(4-pyridinyl)-l-piperazinyl]carbonyl]pentyl]amino]-1- [(3,5-dibromo-4-hydroxyphenyl)methyl]-2-oxoethyl]-4-(1,4-dihydro-2-oxo-3(2 H)-quinazolinyl) (BIBN4096BS) affinity for calcitonin gene-related peptide and amylin receptors–the role of receptor activity modifying protein 1. Mol. Pharmacol. *70*, 1984–1991.

Hilairet, S., Foord, S.M., Marshall, F.H., and Bouvier, M. (2001). Protein-protein interaction and not glycosylation determines the binding selectivity of heterodimers between the calcitonin receptor-like receptor and the receptor activity-modifying proteins. J. Biol. Chem. *276*, 29575–29581.

Ho, T.W., Ferrari, M.D., Dodick, D.W., Galet, V., Kost, J., Fan, X., Leibensperger, H., Froman, S., Assaid, C., Lines, C., et al. (2008a). Efficacy and tolerability of MK-0974 (telcagepant), a new oral antagonist of calcitonin gene-related peptide receptor, compared with zolmitriptan for acute migraine: a randomised, placebo-controlled, parallel-treatment trial. Lancet *372*, 2115–2123.

Ho, T.W., Mannix, L.K., Fan, X., Assaid, C., Furtek, C., Jones, C.J., Lines, C.R., and Rapoport, A.M. (2008b). Randomized controlled trial of an oral CGRP receptor antagonist, MK-0974, in acute treatment of migraine. Neurology *70*, 1304–1312.

Ittner, L.M., Koller, D., Muff, R., Fischer, J.A., and Born, W. (2005). The N-terminal extracellular domain 23-60 of the calcitonin receptor-like receptor in chimeras with the parathyroid hormone receptor mediates association with receptor activity-modifying protein 1. Biochemistry *44*, 5749–5754.

Koller, D., Born, W., Leuthauser, K., Fluhmann, B., McKinney, R.A., Fischer, J.A., and Muff, R. (2002). The extreme N-terminus of the calcitonin-like receptor contributes to the selective interaction with adrenomedullin or calcitonin gene-related peptide. FEBS Lett. *531*, 464–468.

Koth, C.M., Abdul-Manan, N., Lepre, C.A., Connolly, P.J., Yoo, S., Mohanty, A.K., Lippke, J.A., Zwahlen, J., Coll, J.T., Doran, J.D., et al. (2010). Refolding and characterization of a soluble ectodomain complex of the calcitonin gene-related Peptide receptor. Biochemistry *49*, 1862–1872.

Kusano, S., Kukimoto-Niino, M., Akasaka, R., Toyama, M., Terada, T., Shirouzu, M., Shindo, T., and Yokoyama, S. (2008). Crystal structure of the human receptor activity-modifying protein 1 extracellular domain. Protein Sci. *17*, 1907–1914.

Kuwasako, K., Kitamura, K., Nagoshi, Y., Cao, Y.N., and Eto, T. (2003). Identification of the human receptor activity-modifying protein 1 domains responsible for agonist binding specificity. J. Biol. Chem. *278*, 22623–22630.

Lassen, L.H., Haderslev, P.A., Jacobsen, V.B., Iversen, H.K., Sperling, B., and Olesen, J. (2002). CGRP may play a causative role in migraine. Cephalalgia *22*, 54–61.

Link, A.S., Kuris, A., and Edvinsson, L. (2008). Treatment of migraine attacks based on the interaction with the trigemino-cerebrovascular system. J. Headache Pain *9*, 5–12.

Mallee, J.J., Salvatore, C.A., LeBourdelles, B., Oliver, K.R., Longmore, J., Koblan, K.S., and Kane, S.A. (2002). Receptor activity-modifying protein 1 determines the species selectivity of non-peptide CGRP receptor antagonists. J. Biol. Chem. *277*, 14294–14298.

McLatchie, L.M., Fraser, N.J., Main, M.J., Wise, A., Brown, J., Thompson, N., Solari, R., Lee, M.G., and Foord, S.M. (1998). RAMPs regulate the transport and ligand specificity of the calcitonin-receptor-like receptor. Nature *393*, 333–339.

Miller, P.S., Barwell, J., Poyner, D.R., Wigglesworth, M.J., Garland, S.L., and Donnelly, D. (2010). Non-peptidic antagonists of the CGRP receptor, BIBN4096BS and MK-0974, interact with the calcitonin receptor-like receptor via methionine-42 and RAMP1 via tryptophan-74. Biochem. Biophys. Res. Commun. *391*, 437–442.

Moore, E.L., Burgey, C.S., Paone, D.V., Shaw, A.W., Tang, Y.S., Kane, S.A., and Salvatore, C.A. (2009). Examining the binding properties of MK-0974: A CGRP receptor antagonist for the acute treatment of migraine. Eur. J. Pharmacol. *602*, 250–254.

Olesen, J., Diener, H.C., Husstedt, I.W., Goadsby, P.J., Hall, D., Meier, U., Pollentier, S., and Lesko, L.M. (2004). Calcitonin gene-related peptide receptor antagonist BIBN 4096 BS for the acute treatment of migraine. N. Engl. J. Med. *350*, 1104–1110.

Paone, D.V., Shaw, A.W., Nguyen, D.N., Burgey, C.S., Deng, J.Z., Kane, S.A., Koblan, K.S., Salvatore, C.A., Mosser, S.D., Johnston, V.K., et al. (2007). Potent, orally bioavailable calcitonin gene-related peptide receptor antagonists for the treatment of migraine: discovery of N-[(3R,6S)-6-(2,3-difluorophenyl)-2-oxo-1- (2,2,2-trifluoroethyl)azepan-3-yl]-4- (2-oxo-2,3-dihydro-1H-imidazo[4,5-b]pyridin- 1-yl)piperidine-1-carboxamide (MK-0974). J. Med. Chem. *50*, 5564–5567.

Parthier, C., Kleinschmidt, M., Neumann, P., Rudolph, R., Manhart, S., Schlenzig, D., Fanghanel, J., Rahfeld, J.U., Demuth, H.U., and Stubbs, M.T. (2007). Crystal structure of the incretin-bound extracellular domain of a G protein-coupled receptor. Proc. Natl. Acad. Sci. USA *104*, 13942–13947.

Pioszak, A.A., Parker, N.R., Suino-Powell, K., and Xu, H.E. (2008). Molecular recognition of corticotropin-releasing factor by its G-protein-coupled receptor CRFR1. J. Biol. Chem. *283*, 32900–32912.

Pioszak, A.A., and Xu, H.E. (2008). Molecular recognition of parathyroid hormone by its G protein-coupled receptor. Proc. Natl. Acad. Sci. USA *105*, 5034–5039.

Rudolf, K., Eberlein, W., Engel, W., Pieper, H., Entzeroth, M., Hallermayer, G., and Doods, H. (2005). Development of human calcitonin gene-related peptide (CGRP) receptor antagonists. 1. Potent and selective small molecule CGRP antagonists. 1-[N2-[3,5-dibromo-N-[[4-(3,4-dihydro-2(1H)-oxoquinazolin-3-yl)-1-piperidi nyl]carbonyl]-D-tyrosyl]-l-lysyl]-4-(4-pyridinyl)piperazine: the first CGRP antagonist for clinical trials in acute migraine. J. Med. Chem. *48*, 5921–5931.

Runge, S., Thogersen, H., Madsen, K., Lau, J., and Rudolph, R. (2008). Crystal structure of the ligand-bound glucagon-like peptide-1 receptor extracellular domain. J. Biol. Chem. *283*, 11340–11347.

Salvatore, C.A., Mallee, J.J., Bell, I.M., Zartman, C.B., Williams, T.M., Koblan, K.S., and Kane, S.A. (2006). Identification and pharmacological characterization of domains involved in binding of CGRP receptor antagonists to the calcitonin-like receptor. Biochemistry *45*, 1881–1887.

Salvatore, C.A., Hershey, J.C., Corcoran, H.A., Fay, J.F., Johnston, V.K., Moore, E.L., Mosser, S.D., Burgey, C.S., Paone, D.V., Shaw, A.W., et al. (2008). Pharmacological characterization of MK-0974 [N-[(3R,6S)-6-(2,3-difluorophenyl)-2-oxo-1-(2,2,2-trifluoroethyl)azepan-3- yl]-4-(2-oxo-2,3-dihydro-1H-imidazo[4,5-b]pyridin-1-yl)piperidine-1-carbox amide], a potent and orally active calcitonin gene-related peptide receptor antagonist for the treatment of migraine. J. Pharmacol. Exp. Ther. *324*, 416–421.

Schindler, M., and Doods, H.N. (2002). Binding properties of the novel, non-peptide CGRP receptor antagonist radioligand, [(3)H]BIBN4096BS. Eur. J. Pharmacol. *442*, 187–193.

Shaw, A.W., Paone, D.V., Nguyen, D.N., Stump, C.A., Burgey, C.S., Mosser, S.D., Salvatore, C.A., Rutledge, R.Z., Kane, S.A., Koblan, K.S., et al. (2007). Caprolactams as potent CGRP receptor antagonists for the treatment of migraine. Bioorg. Med. Chem. Lett. *17*, 4795–4798.

Stump, C.A., Bell, I.M., Bednar, R.A., Bruno, J.G., Fay, J.F., Gallicchio, S.N., Johnston, V.K., Moore, E.L., Mosser, S.D., Quigley, A.G., et al. (2009). The discovery of highly potent CGRP receptor antagonists. Bioorg. Med. Chem. Lett. *19*, 214–217.

Sun, C., Song, D., Davis-Taber, R.A., Barrett, L.W., Scott, V.E., Richardson, P.L., Pereda-Lopez, A., Uchic, M.E., Solomon, L.R., Lake, M.R., et al. (2007). Solution structure and mutational analysis of pituitary adenylate cyclase-activating polypeptide binding to the extracellular domain of PAC1-RS. Proc. Natl. Acad. Sci. USA *104*, 7875–7880.

Theberge, C.R., Bednar, R.A., Bell, I.M., Corcoran, H.A., Fay, J.F., Hershey, J.C., Johnston, V.K., Kane, S.A., Mosser, S., Salvatore, C.A., et al. (2008). Potent benzimidazolone-based CGRP receptor antagonists. Bioorg. Med. Chem. Lett. *18*, 6122–6125.